Journal of Molecular Graphics and Modelling 29 (2010) 406–414

Contents lists available at ScienceDirect

Journal of Molecular Graphics and Modelling

journal homepage: www.elsevier.com/locate/JMGM

Structural and dynamic features of apolipoprotein A-I cysteine mutants, Milano and Paris, in synthetic HDL

Alessandro Guerini Rocco, Cristina Sensi, Elisabetta Gianazza, Laura Calabresi, Guido Franceschini, Cesare R. Sirtori, Ivano Eberini*

Dipartimento di Scienze Farmacologiche, Università degli Studi di Milano, via Balzaretti 9, 20133 Milano, Italy

ARTICLE INFO

Article history:
Received 4 May 2010
Received in revised form 29 July 2010
Accepted 5 August 2010
Available online 20 August 2010

Keywords:
Apolipoprotein A-I
Mutation
Computer simulation
Molecular models
Lipoproteins
Protein structure

ABSTRACT

Pursuing an established research interest in our group, we built two models for synthetic HDL containing the natural cysteine mutants of apolipoprotein A-I, apolipoprotein A-I Milano (apoA-IM) and apolipoprotein A-I Paris (apoA-IP), both in their homodimeric form. Data on the structural and dynamic properties of such s-HDL are an essential preliminary step for the understanding of the biological activity of the two mutants. Furthermore, comparison between apoA-IM and apoA-IP allows evaluating the effects of the same mutation in a different position in the primary structure and to directly compare our findings with previously published models. We computed for 50 ns in explicit solvent the molecular dynamics of the two complexes and analyzed different properties as a function of time. The proposed s-HDL structures differ significantly from one another and from wild type apolipoprotein A-I. All features of the apoA-IM model are consistent with experimental data. The higher RMSF of apoA-IM has a counterpart in the finding that trypsin, matrix metalloproteases, and chymase degrade apoA-IM much faster than wild type apoA-I; the primary cutting site is correctly identified by molecular dynamics data on our model of apoA-IM-containing s-HDL. The few experimental data for apoA-IP prevent direct comparison with our findings.

1. Introduction

Experience with synthetic high-density lipoproteins (s-HDL) has proven that the anti-atherogenic, anti-thrombotic and anti-inflammatory properties of natural HDL (reviewed in [1,2]) rest on their main protein component, apolipoprotein A-I (apoA-I). A number of apoA-I mutants have been characterised [3–5]. While most of them are linked with pathological phenotypes (e.g. deletion [6], non-conservative [7], nonsense [8], frameshift [9]), two variants, apoA-I Milano (apoA-IM) [10] and apoA-I Paris (apoA-IP) [11], appear to exhibit some unique, favourable features [10,12]. A common structural feature of the two variants is the presence of an arginine-to-cysteine mutation, at amino acid 173 in Milano and 151 in Paris. This leads to the formation of homodimers (apoA-IM–apoA-IM; apoA-IP–apoA-IP) and heterodimers with apoA-II (apoA-IM–apoA-II; apoA-IP–apoA-II).

Carriers of both mutants (all of them heterozygous) have low levels of circulating HDL [13]; in contrast to their hypo-α-cholesterolemic phenotype, however, apoA-IM carriers do not differ to any extent in the entity of carotid intima-media thickness with respect to close relatives living in the same environment and with HDL levels in the normal range [14]. For both apoA-I variants a gain-of-function has been reported in their being able to prevent lipoxygenase-mediated phospholipids oxidation (apoA-IM > apoA-IP), whereas wild type apoA-I is poorly active in this respect [15]. Cholesterol-effluxing capacity has been investigated only for apoA-IM: small r-HDL (7.8 nm in diameter) containing apoA-IM–apoA-IM are more efficient than the corresponding wild type apoA-I particles as acceptors of cell membrane cholesterol. Large particles (12.5 nm in diameter), either with wild type apoA-I or apoA-IM, are instead equivalent in their cholesterol-effluxing capacity [16]. Previous data on apoA-IM published by our research group [17,18] suggested that the sensitivity to proteases, which is higher for the apoAIM–apoA-II heterodimer and the apoA-IM–apoA-IM homodimer than for wild type apoA-I, could be a further protective mechanism of this natural mutant. ApoA-IM could enter the artery wall from circulation, acting as a decoy substrate for plaque proteases, thus exerting a protective effect against plaque rupture.

To make sense of the specific features of the mutants, structure–function relationships need to be investigated on a molecular model of the proteins at atomic resolution. With their

Abbreviations: apoA-I, apolipoprotein A-I; apoA-IM, apolipoprotein A-I Milano; apoA-IP, apolipoprotein A-I Paris; DMPC, dimyristoylphosphatidylcholine; EM, energy minimisation; FFT, fast Fourier transform; HDL, high-density lipoproteins; LCAT, lecithin-cholesterol acyltransferase; MD, molecular dynamics; PME, particle-mesh Ewald; POPC, palmitoyloleoyl phosphatidylcholine; RMS, root mean-square; SA, simulated annealing; SAS, solvent accessible area.

* Corresponding author. Tel.: +39 02 50318256; fax: +39 02 50318284.
E-mail address: ivano.eberini@unimi.it (I. Eberini).

1093-3263/$ – see front matter © 2010 Elsevier Inc. All rights reserved.
doi:10.1016/j.jmgm.2010.08.002

amphipathic nature, apolipoproteins are natively folded only in a hydrophobic environment, i.e. when bound to lipids inside the lipoprotein particles [19]. Between amino acid 44 and 243 the secondary structure of apoA-I is composed of ten amphipathic α-helices, punctuated at regular intervals by proline residues [20,21]. The tertiary structure is known at atomic resolution only for lipid-free apoA-I based on a crystal structure published in 1997 [22]. Because of the lack of structural data at atomic resolution on apoA-I in HDL, several models for the three-dimensional structure of such an assembly have been proposed (see a recent review in [23]). The published models have been obtained through computational [24–26], experimental [27,28], or combined approaches [29,30]. Often the proposed structures differ in several respects, and it is quite difficult to sum-up all features in a single model to envision a 'global prophesy'. Even methods based on the direct observations of apoA-I in synthetic discoidal HDL gave conflicting results: Wu et al. [30] proposed a double superhelix structure from small angle neutron scattering data supported by mass spectrometry, whereas Culot et al. [31] observed a picket-fence arrangement by scanning tunnelling microscopy. However none of these approaches has a resolution adequate to solve apoA-I structure at atomic level, which makes the proposed models inadequate for molecular mechanics studies. Moreover, in both natural mutants in this investigation the formation of a covalent cystine bond between the mutated amino acids induces relevant structural constraints, which are not compatible with some of the models proposed for wild type apoA-I. Conversely, the structural restraints present in the homodimeric forms of apoA-IM and apoA-IP have been used to validate the most credited of these models, the double belt, and to extend its applicability [32].

With an approach similar to our modelling of s-HDL containing wild type apoA-I [26], in the present investigation we made direct reference to the published crystal structure of apoA-I, and applied computational procedures to model the homodimeric forms of apoA-IM and apoA-IP. The available crystal could only be solved at low resolution (4.0 Å) [22]. We already discussed thoroughly [26] why we maintain that the use of such structure implies some obvious approximations, but no real limitation to our computational work.

We next built the models of two s-HDL, containing one molecule each of either apoA-IM–apoA-IM or of apoA-IP–apoA-IP, together with a homogeneous phospholipid bilayer of L-α-palmitoyloleoyl phosphatidylcholine (POPC). We then computed for 50 ns in explicit solvent the MD simulations of the two macromolecular complexes to obtain data on their structural and dynamic properties. Such MD results are an essential preliminary step for the understanding of the biological activity of the two mutants. Furthermore, comparison between apoA-IM and apoA-IP allows evaluating the effects of the same mutation in a different position in the primary structure and to directly compare our findings with previously published models.

2. Materials and methods

2.1. Preparation of the apoA-IM and apoA-IP molecules

ApoA-IM and apoA-IP were obtained introducing, respectively, the R173C and the R151C mutations in both A and B chains of wild type apoA-I (PDB ID code: 1AV1, chains A and B, both corresponding to amino acids 44–243 of the protein primary structure) with the Biopolymer module of the Insight II suite (Accelrys, San Diego, CA). The rotamer library for cysteine was then manually explored and the most favourable energetic arrangements were selected. In agreement with previous data [33,34], the lack of the N-terminal domain of apoA-I is not expected to influence the formation of small s-HDL.

2.2. Preparation of the apoA-IM–apoA-IM and apoA-IP–apoA-IP homodimers

ApoA-IM and apoA-IP were docked to another copy of themselves by using the rigid docking approach implemented in ZDOCK with default parameters, generating 2000 solutions for each A–A′, A–B and B–B′ chain pairs. The 20 solutions with lowest energy were visually inspected. Only the complexes with a cysteine sulphur–sulphur distance compatible with cystine formation after EM were accepted. The selected complexes were subjected to energy minimisation (EM) with MOE (Chemical Computing Group, Quebec, Canada), using the CHARMM27 force field, down to a root mean-square (RMS) gradient of 0.001 kcal mol^{-1} Å^{-1};a distance-dependent dielectric term ($e = 4r$) was applied, as in Vitale et al. [35]. The structures of apoA-IM–apoA-IM and of apoA-IP–apoA-IP with the lowest energy were used to set up the system for the two main MD simulations.

2.3. Preparation of the s-HDL particles and MD simulations

The preparation of the s-HDL particles containing the homodimeric forms of apoA-IM or apoA-IP required a large and equilibrated double layer of POPC: an equilibrated 32×32 lipid-molecule bilayer was obtained from the free-access database of bilayer structures of Peter Tieleman (http://moose.bio.ucalgary.ca/) and used to manually create a larger bilayer of 64×64 POPC molecules. This novel membrane structure was energy-minimised, solvated with water in a $16 \times 16 \times 16$ nm^3 box, and minimised again; then its dynamics was simulated for 2 ns to get an equilibrated structure and to avoid any boundary artefact. The apoA-IM–apoA-IM and the apoA-IP–apoA-IP molecules were placed into the double layer while getting as many lipid molecules as possible trapped into the hole formed by the ringlike dimer structure, in agreement with relevant experimental data on the s-HDL composition [36]. The lipid molecules remaining outside the hole were manually removed using the Insight II suite, running on SGI Fuel, with the aid of Stereo Graphics Crystal Eyes stereo view. The resulting s-HDL particle with the apoA-IM–apoA-IM homodimer contained 98 POPC molecules; it was inserted in a $16 \times 16 \times 16$ nm^3 box, and neutralised with 14 Na^+ ions. The s-HDL particle with the apoA-IP–apoA-IP homodimer contained 94 POPC molecules; it was inserted in a $15 \times 15 \times 15$ nm^3 box, and neutralised with 14 Na^+ ions. Both systems were solvated with the simple point charge model of water. After an initial energy minimisation, they were simulated in two different steps: (1) 1 ns of position-restrained MD with an isotropic force (1000 kJ mol^{-1} nm^{-2}) applied to all protein atoms to allow for both water exit from the hydrophobic bilayer core and solvent relaxation; and (2) 50 ns of unrestrained MD. The GROMOS96 force field, modified according to Berger et al. [37] to improve lipid properties, was applied. All the simulations were performed at 300 K and 1 bar with a coupling constant of 0.1 ps for temperature and 1.0 ps for pressure, in both cases applying the Berendsen weak coupling algorithms [38]. The time step for integration was set at 2 fs. Fast particle-mesh Ewald (PME) electrostatics [39,40] was applied with the following parameters: distance for the Lennard–Jones cutoff = 0.9 nm; distance for the Coulomb cutoff = 0.9 nm; maximum spacing for the fast Fourier transform (FFT) grid = 0.12 nm and a cubic interpolation order, with neighbour list searching (updated every 10 steps). The main simulations were carried out on the Vital-IT Linux cluster at Lausanne.

2.4. Simulation of apoA-IP–apoA-IP with wall restraints

Simulated annealing (SA) of two models of s-HDL containing apoA-IP–apoA-IP and POPC with either parallel or antiparallel arrangements were carried out. A s-HDL model containing two

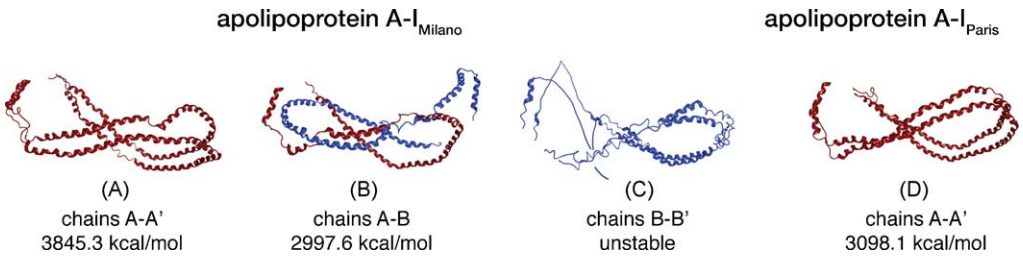

Fig. 1. Molecular configurations and potential energies after EM for the geometrically acceptable structures of the apoA-IM–apoA-IM (panels A–C) and apoA-IP–apoA-IP homodimers (panel D) obtained by ZDOCK. The protein structures are rendered as α-carbon ribbons. A/A′ (in red) and B/B′ (in blue) refer to chains A and B of 1AV1 structure in RCSB PDB. (For interpretation of the references to color in the figure caption, the reader is referred to the web version of the article.)

molecules of wild type apoA-I in an antiparallel arrangement, published by Segrest et al. [41], was taken as starting point. The R151C mutation was introduced in both the apoA-I molecules, then one of the chains was rotated around the common central axis till distance and relative orientation were suitable for the formation of the cystine disulfide bond in an antiparallel model. Conversely, to obtain the parallel model, one of the two apoA-IP molecules was flipped around its major axis before the rotation that would allow for the cystine disulfide bond. Usually, simulations of phospholipid particles need to be carried out with explicit solvent models, since hydrostatic pressure of water is necessary to keep them in place and prevent diffusion in the simulation box. In order to carry out SA with an implicit solvent model, a wall restraint was applied to the POPC molecules. The restraint fundamental function form is:

$$p(t) = \begin{cases} |0 & \text{if } t < 0 \\ |t^3(6 - 8t + 3t^2) & \text{if } t \text{ in } [0, 1] \\ |t & \text{if } t > 1 \end{cases}$$

which is used with t set to various values to achieve the restraint conditions. The function p is twice continuously differentiable since $p'(0) = 0$, $p'(1) = 1$ and $p''(0) = p''(1) = 0$. The wall restraint enclosed all the phospholipids of our models inside an ellipsoidal space; the phospholipid atoms were restrained to lie in an axis-aligned region. For an atom with coordinates (x, y, z) the ellipsoidal restraint energy E_w is given by

$$E_w = Wp(R - 1)$$

$$R = \text{sqrt}\left(\left[\frac{x - x_0}{D_x}\right]^2 + \left[\frac{y - y_0}{D_y}\right]^2 + \left[\frac{z - z_0}{D_z}\right]^2\right)$$

where D defines the radii along each axis. The CHARMM27 force field was used with an implicit reaction field solvent model. After an energy minimisation step down to a root mean-square of 0.00001 kcal mol^{-1} Å^{-1}, the SA protocol consisted of 3 different steps: (1) heating from 0 to 500 K in 100 ps, (2) production at 500 K for 2 ns, (3) cooling from 500 to 0 K in 100 ps. At the end of the SA, the potential energies of the two simulated systems were measured and compared.

3. Results and discussion

First, we like to remind that no structure at atomic resolution is available for apoA-I embedded in a lipid bilayer. Although the assignment of NMR resonances has recently been completed for the backbone of human apolipoprotein AI in a 38 kDa preβ-HDL particle [42], no three-dimensional model based on these data has been released. Crystallization of the lipid-free Δ43-apolipoprotein resulted in a multimeric assembly whose structure could be characterized at 4 Å resolution [22]. The apoA-I model obtained by small angle neutron scattering [30] was made available only when our calculations were concluded, and with resolution lower than by X-ray crystallography.

3.1. Protein chain–protein chain docking

In Fig. 1 the configurations and the potential energies after EM are reported for the geometrically acceptable structures of the apoA-IM–apoA-IM (Fig. 1, panels A–C) and apoA-IP–apoA-IP homodimers (Fig. 1, panel D) obtained by ZDOCK from *in silico* mutated wild type apoA-I chains in their crystal conformation. The top-scoring solution for the apoA-IM homodimers contains the apolipoprotein molecules in an antiparallel arrangement (Fig. 1, panel B). This result is consistent with all experimental and computational data on apoA-I or apoA-IM structure [23,26,32]. On the contrary, the only acceptable solution for apoA-IP homodimers shows a parallel arrangement of the protein chains (Fig. 1, panel D); none of the 20 best scoring solutions involved an antiparallel arrangement. Structural data about apoA-IP are scanty, and only one paper has been published with a proposed model [32]. In that computational report, the authors emphasise the contribution of salt bridges in determining the arrangement of the apolipoprotein chains, both apoA-I and apoA-IM/apoA-IP in their homodimeric forms. In detail, they evaluate the weighted salt bridge scores of the docking interface for wild type apoA-I and for its natural mutants. From their data, salt bridges appear to contribute a substantial stabilisation to the antiparallel forms of apoA-I, apoA-IM, and apoA-IP.

3.2. Simulation of apoA-IP–apoA-IP in implicit solvent with wall restraints

To take care of this apparent inconsistency, before running the main simulation on our s-HDL model containing the parallel homodimeric apoA-IP, we carried out two test MD, taking as starting point the model proposed in [41] for wild type apoA-I and modifying it as detailed in Section 2. Since the antiparallel arrangement of apoA-IP chains had been accounted for only on the basis of the salt bridge score [32], our aim was to investigate in depth the contributions of all the other energetic components involved in the two alternative arrangements. In these test simulations we used a SA protocol and applied a wall restraint potential to the phospholipid molecules. The presence of a wall restraint was to allow the use of an implicit solvent model, both avoiding phospholipid diffusion even in the absence of hydrostatic pressure and speeding up the simulations. With the SA protocol we meant to remove any structural bias that might have been introduced during the manual steps of s-HDL set-up containing either the parallel or the antiparallel forms of apoA-IP. We thus heated the two alternative systems from 0 to 500 K, shortly simulated their behavior at 500 K, and finally cooled them back to 0 K. The energies of the parallel and antiparallel models, evaluated at the end of the simulated annealing in the absence of any kinetic energy, are reported in Table 1. Potential energies of the two systems are very simi-

Table 1
Energies at 0 K after SA of apoA-IP–apoA-IP containing r-HDL models with parallel and antiparallel arrangement of the chains (from [41]) and of their components.

	Potential energy (kcal/mol)	Van der Waals energy (kcal/mol)[a]	Electrostatic energy (kcal/mol)[a]
Antiparallel arrangement			
System	−16.503	−5.901	−22.191
(chain A + chain B)	−7.699	1.003	−13.414
(chain A) vs. (chain B)	−2.442	−209	−2.237
Parallel arrangement			
System	−16.373	−5.898	−22.028
(chain A + chain B)	−7.749	1.006	−13.428
(chain A) vs. (chain B)	−2.638	−213	−2.429

[a] Only the VdW and the electrostatics contributions to s-HDL potential energies are reported and discussed in the manuscript.

lar, and the negative values associated with both the assemblies demonstrate their stability (see 'Potential Energy' column, 'System' lines). Also the very similar potential energy values of the two apoA-IP homodimers (see 'Potential energy' column, 'chain A + chain B' lines) suggest that the parallel and antiparallel arrangements are both energetically possible.

The models we have proposed for s-HDL containing apoA-I::apoA-I [26], apoA-IM–apoA-II [43], and apoA-IM–apoA-IM (this manuscript), but not apoA-IP–apoA-IP, are in agreement with Klon's inference that the contribution of the salt bridges between the two chains is crucial in favour of the antiparallel arrangement [32]. The SA experiments referred to in this section however exclude that the salt bridges are discriminant in defining the relative orientation of apoA-IP chains, and do not invalidate our s-HDL model with apoA-IP in parallel orientation. Also the energetic analysis of the electrostatic interactions between chain A and chain B (see 'Electrostatic energy' column, 'chain A vs. chain B' lines) shows that the inter-helical salt bridges give a similar contribution to both the parallel and antiparallel apoA-IP chain arrangements. All of these findings led us then to regard as fully acceptable the parallel arrangement we had obtained for apoA-IP from the docking step (*above*), and to use its structure for building and simulating in explicit solvent a s-HDL containing apoA-IP in homodimeric form (*below*).

Fig. 2 reports a representative timeframe of the above SA procedure: a hairpin structure is clearly visible, formed by amino acids (aa) 177–190 (helices 7 and 8). This observation has never been reported by other research groups involved in MD simulations of apoA-I. ApoA-I sticking to lipids throughout previous calculations

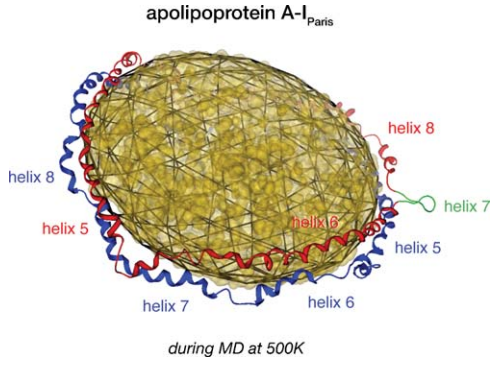

Fig. 2. Structural representation of a s-HDL containing apoA-IP–apoA-IP. This snapshot corresponds to frame 781 ps of a SA simulation having the structure in [41] as starting point. During the SA process, the system was heated from 0 to 500 K in 100 ps, simulated at 500 K for 2 ns and eventually cooled back to 0 K in 100 ps. The simulation was carried out with implicit solvent; wall restraints were applied to phospholipids. The protein structure is rendered as α-carbon ribbon (color code: blue for apoA-I$_{Paris}$, red for apoA-I′$_{Paris}$, green for the putative hinge). The POPC bilayer is rendered as analytic Connolly surface, colored in gold, and surrounding the Van der Walls surface. Wall restraints are represented with a black network. (For interpretation of the references to color in the figure caption, the reader is referred to the web version of the article.)

might be due to the short duration and to the milder simulated conditions: only the high temperature we selected for the production SA step is likely to allow a more efficient exploration of the conformational space. The existence of a hinge region in apoA-I, however, had already been postulated by several authors on the basis of various *in vitro* findings. By spectroscopy Maiorano et al. [44] observed a reduced association with lipophilic reagents for helices 5–7 and hypothesized a 'hinge domain' involving helices 5 and 6 [45,46]; from NMR, Wang et al. [47] reported that amino acids 168–182 (helix 7) are less structured and less lipid-bound than amino acids 142–162 (helices 5 and 6); using hydrogen–deuterium exchange mass spectrometry, Wu et al. provided evidence that residues 159–180 form a protruding solvent-exposed hinge [48]. The residues we identified as forming a hairpin thus partially overlap with the stretches with low affinity for lipids singled out by Wang et al. and by Wu et al. Furthermore, Chetty et al. [49] published hydrogen exchange and mass spectrometry data on lipid-free apoA-I, reporting that the same region we have described as forming a hairpin is placed in a region not associated with a high protection factor; this finding suggests a local structural disorganization, compatible with its peculiar structural features.

The reported protruding loop does not overlap the amino acids directly interacting with LCAT, but is located in a following part of apoA-I sequence. However, mutations in this apoA-I region demonstrated its indirect ability in regulating the interaction with LCAT, and its activation by HDL [50]; this aspect is thoroughly discussed in the following.

3.3. Simulations of s-HDL particles in explicit solvent

Fig. 3 outlines the main steps when building the *in silico* models for s-HDL containing either apoA-IM–apoA-IM or apoA-IP–apoA-IP and a homogeneous POPC bilayer; panels A, B and E, F show the structures of the s-HDL before, panels C, D and G, H after 50 ns of MD.

In the apoA-IM model (panels A–D), the two apolipoprotein chains run antiparallel, without helix 4, 5 or 6 of apoA-IM being associated to the corresponding helix of apoA-IM′ and without pairing between proline residues. This model is very different from the spatial arrangement already reported for apoA-I, i.e. the LL5/5 registration, introduced by Klon et al. [51] and also produced by our modeling procedure for apoA-I::apoA-I [26]. Conversely, in the apoA-IP-containing s-HDL (panels E–H) the two apolipoprotein molecules run parallel, with helices 4, 5, and 6 of apoA-IP associated to the corresponding ones of apoA-IP′. With this arrangement all the pairs of prolines are juxtaposed.

In HDL containing wild type apoA-I, the amino acids implicated in LCAT activation may be arranged in different ways depending on the size of the lipoprotein. In a nascent (small size) HDL the regions from amino acid 139 to 146 (at helix 5 and junction with helix 6) of two apoA-I molecules can organize in a central loop, in which they are close to one another and able to activate LCAT. In

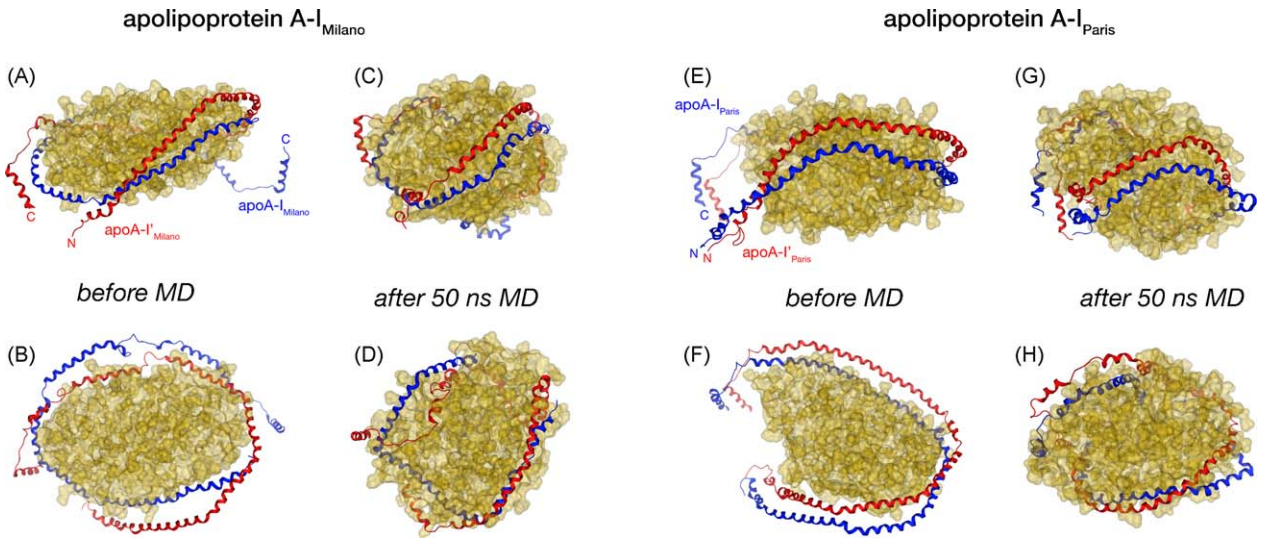

Fig. 3. Structures for s-HDL models containing homodimer apoA-IM–apoA-IM (panels A–D) or apoA-IP–apoA-IP (panels E–H) before and after the MD simulation. On the left: s-HDL with apoA-IM: (A and B) before MD; (C and D) after 50 ns of MD (color code: blue for apoA-IM, red for apoA-IM′). On the right: s-HDL with apoA-IP: (E and F) before MD and (G and H) after 50 ns of MD (color code: blue for apoA-IP, red for apoA-IP′). Protein structures are rendered as α-carbon ribbon. The POPC bilayer is rendered as analytic Connolly surface, colored in gold, and surrounding the Van der Waals surface.

larger HDL the same structural elements are not paired and cannot form the central loop required for the LCAT activity [49]. This peculiar mechanism is useful for regulating cholesterol esterification and HDL metabolism. The formation of a looped belt involving the same amino acids has also been reported in a computational paper by Jones et al. [52]. All these observations can be referred only to wild type apoA-I, whereas in the apoA-I natural mutants containing cystine the same regions are organized in a fixed relative arrangement. Fig. 4 compares the situation of amino acids 143-165 in s-HDL containing either apoA-IM or apoA-IP homodimers. Because of the $^{173}C–^{173}C'$ covalent bond, in apoA-IM the two regions can neither pair nor interact with LCAT. This is consistent with literature data, describing the Milano mutant as a form with an inhibitory effect on LCAT activation [53]. A different arrangement can be observed in apoA-IP, with a tight pairing of the sequences able to interact with LCAT. However, also for the Paris mutant an inhibitory effect on LCAT has been reported, even if minor in comparison with the Milano mutant [54,55]. Both with a parallel and with an antiparallel arrangement, the region 143–165 is well paired in apoA-IP; reduction in LCAT activity could be ascribed to the parallel pairing of these amino acids, as proposed in our model, and/or to the presence inside this region of the $^{151}C–^{151}C'$ covalent bond.

Fig. 5 (panels A–H for apoA-IM, panels I–Q for apoA-IP) shows the evolution with time of the main structural and energetic parameters during the simulations of the two modelled s-HDL. In all cases during the second half of the simulation (from 25 to 50 ns) the monitored values drift over a narrower range and may thus be taken as largely representative of the average structure and behaviour of the s-HDL in solution. The main structural rearrangements observed for both the systems happen in the first part of simulations, with RMSD values starting from approx. 2 nm and reducing to approx. 2 Å at the end (panels A and I of Fig. 5). The relaxation from a solid, lipid-free to a solvated, lipid-bound configuration can be considered almost complete after 25 ns, after which the system dynamics experience only narrower structural modifications. Comparing the structures before and after MD in Fig. 3, it is clear that both apoA-IM and apoA-IP undergo spatial rearrangements that increase the out-of-plane deformation of the starting structures. Specifically, in the apoA-IM-containing s-HDL, the C-terminus of the protein is far

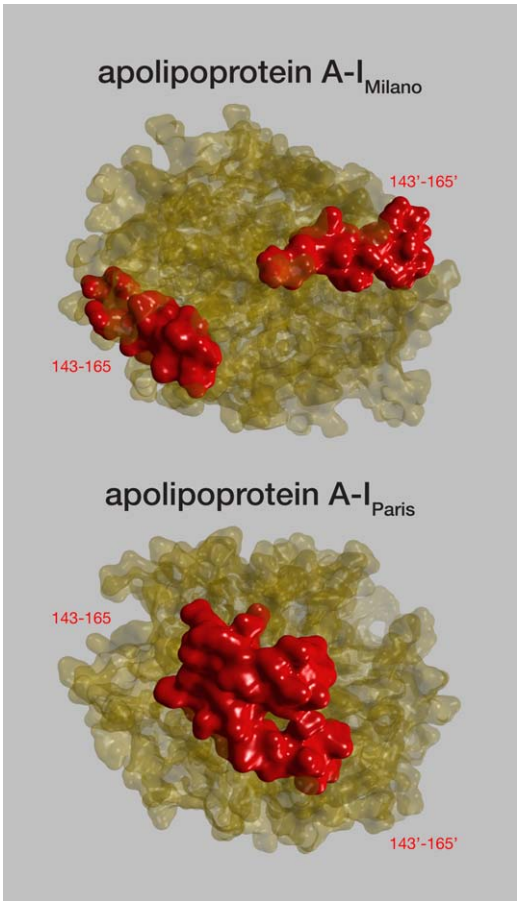

Fig. 4. Relative orientation of the amino acid stretch 143–165 in apoA-IM- and apoA-IP-containing s-HDL. All structural elements are rendered as molecular surface; amino acids 143–165 are colored in red, while the rest of the apoA-I molecules is gray and the phospholipid bilayer is gold. (For interpretation of the references to color in the figure caption, the reader is referred to the web version of the article.)

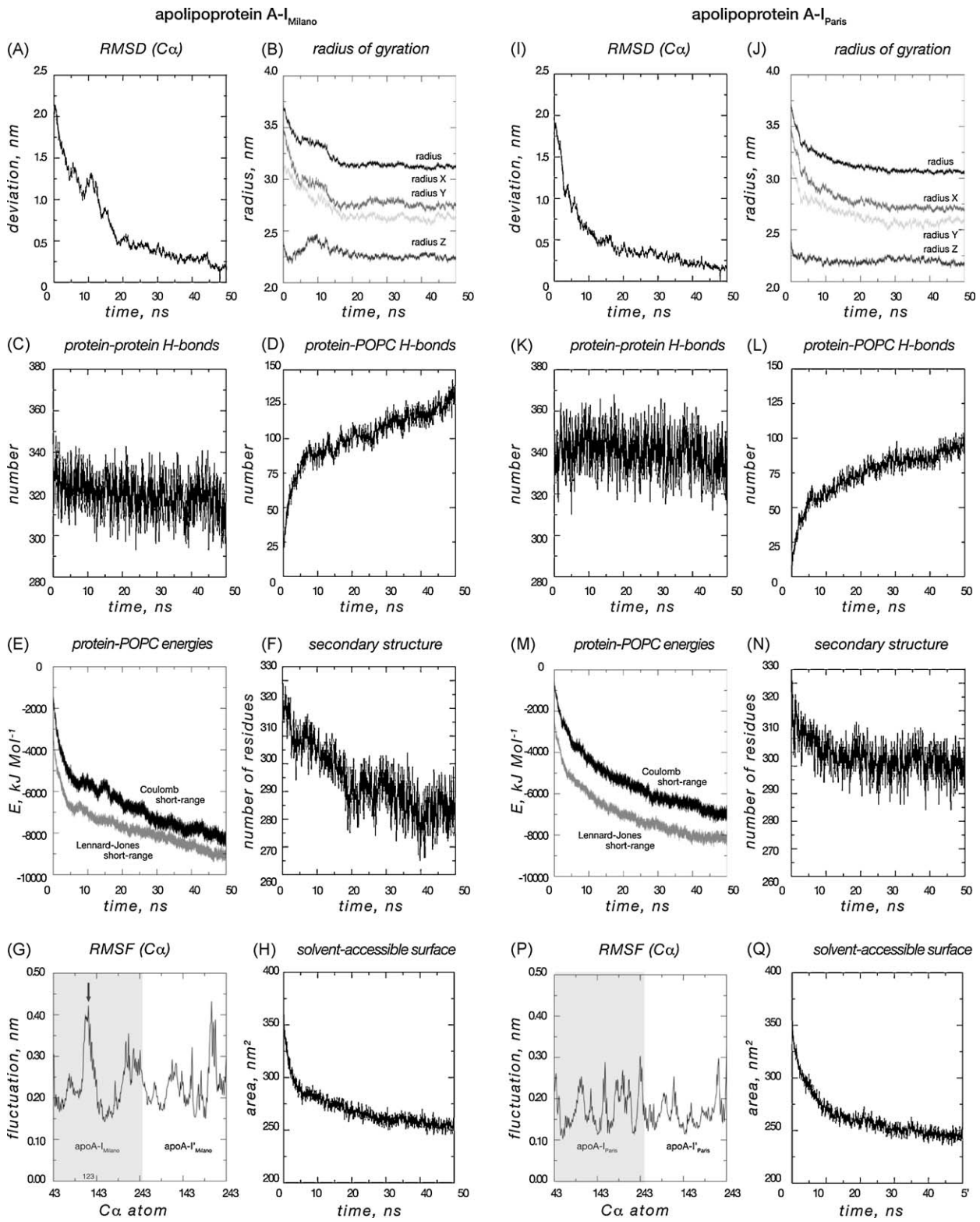

Fig. 5. Structural and energetic parameters for s-HDL models containing homodimer apoA-IM–apoA-IM (panels A–H, on the left) or apoA-IP–apoA-IP (panels I–Q, on the right). (A and I) RMSD computed on α-carbons; (B and J) radius of gyration and its decomposition along cartesian axes; (C and K) number of protein–protein hydrogen bonds; (D and L) number of protein–lipid hydrogen bonds; (E and M) Coulomb short-range and Lennard–Jones short-range protein–lipid interaction energies; (F and N) total number of structured residues; (G and P) RMSF calculated from 25 to 50 ns: amino acid numbering is according to the primary structure of apoA-IM/IP (grey background) and apoA-IM′/IP′ (white background); (H and Q) lipid SAS. The layout of this figure is identical to that in Guerini Rocco et al. [26] for a more direct comparison with the features of the wild type apoA-I-containing s-HDL.

from the POPC core before MD, but during the simulated time it moves towards the lipids, optimising its interaction (Fig. 5, panels D and E). An extensive rearrangement of the protein vs. the phospholipid component is experienced also in the apoA-IP-containing s-HDL (panels L and M). As a result, during MD, both s-HDL particles show a reduction of their gyration radius down to minimal stable values, corresponding to approx. 6.3 nm for apoA-IM, and to 6.1 nm for apoA-IP (Fig. 5, panels B and J, respectively). Considering the *x*, *y* and *z* components of the gyration radius, both s-HDL models show a major and a minor axis: 5.5 nm, and 5.3 nm for apoA-IM containing s-HDL; 5.4 nm, and 5.2 nm for apoA-IP containing s-HDL. These sizes are compatible with the properties of HDL containing apoA-IM, as known from literature data [36]. No POPC molecule is ever lost from either of the s-HDL.

For both protein variants the number of protein–protein hydrogen bonds decreases during the simulations, if only by 3% (Fig. 5, panels C and K); at all times apoA-IP–apoA-IP has a number of hydrogen bonds higher than apoA-IM–apoA-IM (panel K vs. panel C). Accordingly, protein–protein interaction energies only slightly change with simulation time for both s-HDL (not shown). On the contrary, in both s-HDL the number of hydrogen bonds between protein chains and lipids keeps growing with time (panels D and L). In apoA-IM-containing s-HDL, lipid–lipid interaction energies increase slightly in the short-range Coulomb term (not shown), while the short-range Lennard–Jones term only shows small fluctuations (not shown). As a result of the movement of the protein chains towards the POPC core, protein–lipid interaction energies rapidly decrease in the first part of the simulation, strongly reducing its slope at the end of the simulated time for both short-range Coulomb (panel E, black tracing) and Lennard–Jones terms (panel E, grey tracing). The energy behaviour for apoA-IP-containing s-HDL is similar to that of apoA-IM, but an initial remarkable variation is detected in the protein–protein short-range Lennard–Jones component (not shown). These energetic evaluations suggest that the increasing number of favourable interactions between proteins and POPC acts as a major driving force for the structural reorganization and stabilisation of the s-HDL during the simulated time. While the protein chains get closer to the POPC core, the solvent accessible area (SAS) of phospholipids decreases to the same extent for both simulated systems (Fig. 5, panels H and Q).

For both s-HDL the number of amino acids in secondary structure (α-helix) decreases during the MD (Fig. 5, panels F and N) – only slightly for apoA-IP (panel N; 6%) and to a larger extent for apoA-IM (panel F; 12%). As a result, after the 50 ns simulation, apoA-IM-containing s-HDL has an approximately 5% lower content of α-helix than apoA-IP. In addition, both variants have a much lower content of α-helix than wild type apoA-I, in the order of 15–20% (33). A lower content of amino acids in secondary structure is consistent with a higher value of RMSF (Fig. 5, panels G and P) for the protein variants than for wild type apoA-I. In turn, the high flexibility of apoA-IM can explain its peculiar sensitivity to proteolytic enzymes [18,43,56]. When digested *in vitro*, s-HDL, 7.8 nm in diameter, containing the homodimeric form of apoA-IM, yield proteolytic fragments with specific cleavage sites [57]. One of the main enzymatic targets (Arg123-Ala124) is associated in our simulation with the highest RMSF peak (panel G, arrow). Conversely, no cleavage occurs at the same position in wild type apoA-I contained in s-HDL with a 7.8 nm diameter [57].

A DSSP run on the minimised last timeframe of the MD run on the apoA-IM-containing s-HDL detects 300 amino acids in α-helix, out of a total of 400 in the truncated 44–243 chains in the model. Without making any correction for the possible contribution of the 1–43 residues, out of a total of 486 residues in the full-length apolipoproteins this figure would correspond to 75% of the amino acids in secondary structure. Calabresi et al. [58] measured for apoA-IM–apoA-IM in DMPC a molar mean residue ellipticity of −25,670, with an associated α-helix content of 77%, in very close agreement with our computed estimation.

Table 2
Intermolecular salt bridges that remain at an average distance ≤0.35 nm from 25 to 50 ns.

apoA-IM–apoA-IM′		apoA-IP–apoA-IP′	
R^{61}	D^{89}	D^{89}	K^{88}
D^{157}	K^{195}	E^{78}	K^{77}
D^{51}	K^{96}	E^{111}	K^{106}
E^{183}	R^{171}	K^{182}	E^{179}
K^{226}	E^{128}	K^{195}	E^{191}
		K^{118}	E^{113}
		E^{125}	R^{131}
		K^{94}	E^{91}

Table 2, column 1, lists the salt bridges computed from 25 to 50 ns between the two apoA-IM chains, column 2, between the two apoA-IP chains. For both apoA-IM and apoA-IP, none of the salt bridges identified involves the same partners as in the wild type apoA-I model [26]. This finding is not surprising, especially if we consider that the cystine link constrains a specific relative registration of the two protein chains, resulting in different charge pairings.

4. Conclusions

As we have reported above, plenty of experimental data have been published on the issue of apoA-I structure. Several of the published approaches (chemical cross-linking [27,59]; energy transfer fluorescence [60,61]; calorimetry [62]) were aimed at the identification of constraints in wild type apoA-I, to clarify the spatial relationships among some of the amino acids of its sequence. These data have been connected not only to the intrachain arrangement of apoA-I amino acids, but also to the interchain interactions in (synthetic) HDL. Due to the constraining effect of cystine covalent bonds present at different positions, the natural mutants we considered in this study differ in the relative arrangement of the apoA-I chains. Furthermore, it has been reported that the single point mutation occurring both in apoA-IM and apoA-IP has also heavy structural effects on the intrachain spatial organization [63].

Only one model has been published in the literature for each of the mutant apoA-I homodimers, apoA-IM–apoA-IM and apoA-IP–apoA-IP [32]; both use as common basis the same wild type apoA-I model [41]. As a result of this approach, the three structures are very similar to one another. In detail, the way apoA-I chains get in contact is in all cases by antiparallel pairing. For wild type apoA-I the antiparallel orientation was estimated the more stable on the basis of salt bridge and charge apposition score; this observation was extended to the apoA-IM and apoA-IP models [32,41]. In their paper, however, Klon et al. [32] did not produce exhaustive evidence to rule out the possibility of the parallel orientation for the apoA-IP homodimer, which was not studied extensively.

Besides the presence of the cystine cross-link in the mutants, the only difference among the three available models is expected to be in the registration of chain alignment. Instead, secondary and tertiary structure of all chains is assumed to be alike, with similar number of amino acids in secondary structure and similar solvent exposure. This structural homogeneity does not help to explain the biological differences among the three protein variants. Conversely, a recent study [64], focused on the structural and functional properties of various natural and artificial apoA-I cysteine mutants, demonstrated that the variant proteins exhibit different structural features and biological activities. These observations are consistent with the hypothesis that the influence of the local environment of mutations propagates to the whole protein chain [64].

The s-HDL we have obtained after protein–protein docking of apoA-I chains in crystal structure with (in this report) or without [26] *in silico* arginine-to-cysteine mutagenesis differ from one another much more extensively than the previously published models. One of the new models, the s-HDL containing apoA-IP–apoA-IP, appears to be stable when the two protein chains pair with a parallel arrangement, in contrast with the antiparallel pairing of the other two s-HDL.

All the properties that may be inferred from the mutant s-HDL models we have obtained are in good agreement with experimental data. Specifically, this is the case for *in vitro* susceptibility to proteolytic enzymes [43]. RMSF data, both as mean distribution and peak values, differ extensively among the models. Wild type apoA-I appears more rigid [26] than apoA-IP and even more than apoA-IM. The higher RMSF of apoA-IM has a counterpart in the finding that trypsin, matrix metalloproteases, and chymase degrade apoA-IM much faster than wild type apoA-I; no data are available in this respect for apoA-IP. The primary cutting site is correctly identified by MD data on our model of apoA-IM-containing s-HDL.

While computational data can be directly compared with experimental findings for apoA-I and apoA-IM, this is not the case for apoA-IP. ApoA-IP is a natural mutation not as diffused as apoA-IM, since the known apoA-IP carriers do not all live in the same area (as apoA-IM carriers live in Limone sul Garda, Italy). Even though it satisfies all structural and energetic requirements, our proposal for the parallel arrangement of apoA-IP in s-HDL shall require validation through experimental approaches. However, the low number of subjects expressing the Paris mutation restricts experimental procedures based on the purification of apoA-IP.

Acknowledgements

This work was funded in part by MIUR (FIRB 2003: molecular recognition in protein–ligand, protein–protein and protein–surface interactions: development of integrated experimental and computational approaches to the study of systems of pharmaceutical interest). Computational power was provided by the Vital-IT High Performance Computing Center.

References

[1] B.J. Ansell, K.E. Watson, A.M. Fogelman, M. Navab, G.C. Fonarow, High-density lipoprotein function recent advances, J. Am. Coll. Cardiol. 46 (2005) 1792–1798.
[2] M. Navab, R. Yu, N. Gharavi, W. Huang, N. Ezra, A. Lotfizadeh, G.M. Anantharamaiah, N. Alipour, B.J. Van Lenten, S.T. Reddy, D. Marelli, High-density lipoprotein: antioxidant and anti-inflammatory properties, Curr. Atheroscler. Rep. 9 (2007) 244–248.
[3] A. von Eckardstein, H. Funke, M. Walter, K. Altland, A. Benninghoven, G. Assmann, Structural analysis of human apolipoprotein A-I variants: aminoacid substitutions are nonrandomly distributed throughout the apolipoprotein A-I primary structure, J. Biol. Chem. 265 (1990) 8610–8617.
[4] A. Jonas, A. von Eckardstein, K.E. Kezdy, A. Steinmetz, G. Assmann, Structural and functional properties of reconstituted high density lipoprotein discs prepared with six apolipoprotein A-I variants, J. Lipid Res. 32 (1991) 97–106.
[5] A. von Eckardstein, G. Assmann, High density lipoproteins and reverse cholesterol transport: lessons from mutations, Atherosclerosis 137 (Suppl.) (1998) S7–S11.
[6] S.C. Rall Jr., K.H. Weisgraber, R.W. Mahley, Y. Ogawa, C.J. Fielding, G. Utermann, J. Haas, A. Steinmetz, H.J. Menzel, G. Assmann, Abnormal lecithin:cholesterol acyltransferase activation by a human apolipoprotein A-I variant in which a single lysine residue is deleted, J. Biol. Chem. 259 (1984) 10063–10070.
[7] W. Strobl, H.U. Jabs, M. Hayde, T. Holzinger, G. Assmann, K. Widhalm, Apolipoprotein A-I (Glu 198–Lys): a mutant of the major apolipoprotein of high-density lipoproteins occurring in a family with dyslipoproteinemia, Pediatr. Res. 24 (1988) 222–228.
[8] R. Romling, A. von Eckardstein, H. Funke, C. Motti, G.C. Fragiacomo, G. Noseda, G. Assmann, A nonsense mutation in the apolipoprotein A-I gene is associated with high-density lipoprotein deficiency and periorbital xanthelasmas, Arterioscler. Thromb. 14 (1994) 1915–1922.
[9] H. Funke, A. von Eckardstein, P.H. Pritchard, M. Karas, J.J. Albers, G. Assmann, A frameshift mutation in the human apolipoprotein A-I gene causes high density lipoprotein deficiency, partial lecithin: cholesterol-acyltransferase deficiency, and corneal opacities, J. Clin. Invest. 87 (1991) 371–376.
[10] G. Franceschini, C.R. Sirtori, A. Capurso, K.H. Weisgraber, R.W. Mahley, A-I_M apoprotein: decreased high density lipoprotein levels with significant lipoprotein modifications and without clinical atherosclerosis in an Italian family, J. Clin. Invest. 66 (1980) 892–900.
[11] E. Bruckert, A. von Eckardstein, H. Funke, H. Wiebusch, I. Beucler, G. Turpin, G. Assmann, The replacement of arginine by cysteine at residue 151 in apolipoprotein A-I(Paris) causes a phenocopy of apolipoproteinA-I(Milano), Atherosclerosis 128 (1996) 121–128.
[12] G. Franceschini, L. Calabresi, G. Chiesa, C. Parolini, C.R. Sirtori, M. Canavesi, F. Bernini, Increased cholesterol efflux potential of sera from ApoA-I_{Milano} carriers and transgenic mice, Arterioscler. Thromb. Vasc. Biol. 19 (1999) 1257–1262.
[13] G. Franceschini, G. Vecchio, G. Gianfranceschi, D. Magani, C.R. Sirtori, Apolipoprotein A-I_{Milano}: accelerated binding and dissociation from lipids of a human apolipoprotein variant, J. Biol. Chem. 260 (1985) 16321–16325.
[14] C.R. Sirtori, L. Calabresi, G. Franceschini, D. Baldassarre, M. Amato, J. Johansson, M. Salvetti, C. Monteduro, R. Zulli, M. Muiesan, E. Agabiti-Rosei, Cardiovascular status of carriers of the apolipoprotein A-I_{Milano} mutant: the Limone sul Garda study, Circulation 103 (2001) 1949–1954.
[15] J.K. Bielicki, M.N. Oda, Apolipoprotein A-I(Milano) and apolipoprotein A-I(Paris) exhibit an antioxidant activity distinct from that of wild-type apolipoprotein A-I, Biochemistry 41 (2002) 2089–2096.
[16] L. Calabresi, M. Canavesi, F. Bernini, G. Franceschini, Cell cholesterol efflux to reconstituted high-density lipoproteins containing the apolipoprotein A-I_{Milano} dimer, Biochemistry 38 (1999) 16307–16314.
[17] I. Eberini, L. Calabresi, R. Wait, G. Tedeschi, A. Pirillo, L. Puglisi, C.R. Sirtori, E. Gianazza, Macrophage metalloproteinases degrade HDL-associated apoA-I at both the N- and the C-terminus, Biochem. J. 366 (2002) 627–634.
[18] I. Eberini, E. Gianazza, L. Calabresi, C.R. Sirtori, ApoA-I-Milano from structure to clinical application, Ann. Med. 40 (2008) 48–56.
[19] J.P. Segrest, R.L. Jackson, J.D. Morrisett, A.M.J. Gotto, A molecular theory of lipid–protein interactions in the plasma lipoproteins, FEBS Lett. 38 (1974) 247–258.
[20] J.P. Segrest, M.K. Jones, H. De Loof, C.G. Brouillette, Y.V. Venkatachalapathi, G.M. Anantharamaiah, The amphipathic helix in the exchangeable apolipoproteins: a review of secondary structure and function, J. Lipid Res. 31 (1992) 141–166.
[21] M.S. Boguski, M. Freeman, N.A. Elshourbagy, J.M. Taylor, J.I. Gordon, On computer-assisted analysis of biological sequences: proline punctuation, consensus sequences, and apolipoprotein repeats, J. Lipid Res. 27 (1986) 1011–1034.
[22] D.W. Borhani, D.P. Rogers, J.A. Engler, C.G. Brouillette, Crystal structure of truncated human apolipoprotein A-I suggests a lipid-bound conformation, Proc. Natl. Acad. Sci. U.S.A. 94 (1997) 12291–12296.
[23] M.J. Thomas, S. Bhat, M.G. Sorci-Thomas, Three-dimensional models of HDL apoA-I: implications for its assembly and function, J. Lipid Res. 49 (2008) 1875–1883.
[24] A. Catte, J.C. Patterson, M.K. Jones, W.G. Jerome, D. Bashtovyy, Z. Su, F. Gu, J. Chen, M.P. Aliste, S.C. Harvey, L. Li, G. Weinstein, J.P. Segrest, Novel changes in discoidal high density lipoprotein morphology: a molecular dynamics study, Biophys. J. 90 (2006) 4345–4360.
[25] A.Y. Shih, P.L. Freddolino, A. Arkhipov, K. Schulten, Assembly of lipoprotein particles revealed by coarse-grained molecular dynamics simulations, J. Struct. Biol. 157 (2007) 579–592.
[26] A. Guerini Rocco, E. Gianazza, L. Calabresi, C. Sensi, G. Franceschini, C.R. Sirtori, I. Eberini, Structural features and dynamics properties of human apolipoprotein A-I in a model of synthetic HDL, J. Mol. Graph. Model. 28 (2009) 305–312.
[27] R.A. Silva, R. Huang, J. Morris, J. Fang, E.O. Gracheva, G. Ren, A. Kontush, W.G. Jerome, K.A. Rye, W.S. Davidson, Structure of apolipoprotein A-I in spherical high density lipoproteins of different sizes, Proc. Natl. Acad. Sci. U.S.A. 105 (2008) 12176–12181.
[28] B. Chen, X. Ren, T. Neville, W.G. Jerome, D.W. Hoyt, D. Sparks, G. Ren, J. Wang, Apolipoprotein AI tertiary structures determine stability and phospholipid-binding activity of discoidal high-density lipoprotein particles of different sizes, Protein Sci. 18 (2009) 921–935.
[29] F. Gu, M.K. Jones, J. Chen, J.C. Patterson, A. Catte, W.G. Jerome, L. Li, J.P. Segrest, Structures of discoidal high density lipoproteins: a combined computational–experimental approach, J. Biol. Chem. 285 (2010) 4652–4665.
[30] Z. Wu, V. Gogonea, X. Lee, M.A. Wagner, X.M. Li, Y. Huang, A. Undurti, R.P. May, M. Haertlein, M. Moulin, I. Gutsche, G. Zaccai, J.A. Didonato, S.L. Hazen, Double superhelix model of high density lipoprotein, J. Biol. Chem. 284 (2009) 36605–36619.
[31] C. Culot, F. Durant, S. Lazarescu, P.A. Thiry, B. Vanloo, M.Y. Rosseneu, L. Lins, R. Brasseur, Structural investigation of reconstituted high density lipoproteins by scanning tunnelling microscopy, Appl. Surf. Sci. 230 (2004) 151–157.
[32] A.E. Klon, M.K. Jones, J.P. Segrest, S.C. Harvey, Molecular belt models for the apolipoprotein A-I Paris and Milano mutations, Biophys. J. 79 (2000) 1679–1685.
[33] W.S. Davidson, T. Hazlett, W.W. Mantulin, A. Jonas, The role of apolipoprotein AI domains in lipid binding, Proc. Natl. Acad. Sci. U.S.A. 93 (1996) 13605–13610.
[34] L. Li, J. Chen, V.K. Mishra, J.A. Kurtz, D. Cao, A.E. Klon, S.C. Harvey, G.M. Anantharamaiah, J.P. Segrest, Double belt structure of discoidal high density lipoproteins: molecular basis for size heterogeneity, J. Mol. Biol. 343 (2004) 1293–1311.
[35] R.M. Vitale, C. Pedone, P.G. De Benedetti, F. Fanelli, Structural features of the inactive and active states of the melanin-concentrating hormone receptors: insights from molecular simulations, Proteins 56 (2004) 430–448.

[36] L. Calabresi, G. Vecchio, F. Frigerio, L. Vavassori, C.R. Sirtori, G. Franceschini, Reconstituted high-density lipoproteins with a disulfide-linked apolipoprotein A-I dimer: evidence for restricted particle size heterogeneity, Biochemistry 36 (1997) 12428–12433.
[37] O. Berger, O. Edholm, F. Jahnig, Molecular dynamics simulations of a fluid bilayer of dipalmitoylphosphatidylcholine at full hydration, constant pressure, and constant temperature, Biophys. J. 72 (1997) 2002–2013.
[38] H.J.C. Berendsen, J.P.M. Postma, A. DiNola, J.R. Haak, Molecular dynamics with coupling to an external bath, J. Chem. Phys. 81 (1984) 3684–3690.
[39] T. Darden, D. York, L. Pedersen, Particle mesh Ewald: an N-log(N) method for Ewald sums in large systems, J. Chem. Phys. 98 (1993) 10089–10092.
[40] U. Essmann, L. Perera, M.L. Berkowitz, T. Darden, H. Lee, L.G. Pedersen, A smooth particle mesh Ewald potential, J. Chem. Phys. 103 (1995) 8577–8592.
[41] J.P. Segrest, M.K. Jones, A.E. Klon, C.J. Sheldahl, M. Hellinger, H. De Loof, S.C. Harvey, A detailed molecular belt model for apolipoprotein A-I in discoidal high density lipoprotein, J. Biol. Chem. 274 (1999) 31755–31758.
[42] X. Ren, Y. Yang, T. Neville, D. Hoyt, D. Sparks, J. Wang, A complete backbone spectral assignment of human apolipoprotein AI on a 38 kDa prebetaHDL (Lp1-AI) particle, Biomol. NMR Assign. 1 (2007) 69–71.
[43] A. Guerini Rocco, L. Mollica, E. Gianazza, L. Calabresi, G. Franceschini, C.R. Sirtori, I. Eberini, A model structure for the heterodimer apoA-IMilano-apoA-II supports its peculiar susceptibility to proteolysis, Biophys. J. 91 (2006) 3043–3049.
[44] J.N. Maiorano, R.J. Jandacek, E.M. Horace, W.S. Davidson, Identification and structural ramifications of a hinge domain in apolipoprotein A-I discoidal high-density lipoproteins of different size, Biochemistry 43 (2004) 11717–11726.
[45] M.G. Sorci-Thomas, L. Curtiss, J.S. Parks, M.J. Thomas, M.W. Kearns, Alteration in apolipoprotein A-I 22-mer repeat order results in a decrease in lecithin:cholesterol acyltransferase reactivity, J. Biol. Chem. 272 (1997) 7278–7284.
[46] M.G. Sorci-Thomas, L. Curtiss, J.S. Parks, M.J. Thomas, M. Kearns, M. Landrum, The hydrophobic face orientation of apolipoprotein A-I amphipathic helix domain 143–164 regulates lecithin: cholesterol acyltransferase activation, J. Biol. Chem. 273 (1998) 11776–11782.
[47] G.S. Wang, J.T. Sparrow, R.J. Cushley, The helix-hinge-helix structural motif in human apolipoprotein A-I determined by NMR spectroscopy, Biochemistry 36 (1997) 13657–13666.
[48] Z. Wu, M.A. Wagner, L. Zheng, J.S. Parks, J.M. Shy 3rd, J.D. Smith, V. Gogonea, S.L. Hazen, The refined structure of nascent HDL reveals a key functional domain for particle maturation and dysfunction, Nat. Struct. Mol. Biol. 14 (2007) 861–868.
[49] P.S. Chetty, L. Mayne, S. Lund-Katz, D. Stranz, S.W. Englander, M.C. Phillips, Helical structure and stability in human apolipoprotein A-I by hydrogen exchange and mass spectrometry, Proc. Natl. Acad. Sci. U.S.A. 106 (2009) 19005–19010.
[50] K.H. Cho, D.M. Durbin, A. Jonas, Role of individual amino acids of apolipoprotein A-I in the activation of lecithin: cholesterol acyltransferase and in HDL rearrangements, J. Lipid Res. 42 (2001) 379–389.
[51] A.E. Klon, J.P. Segrest, S.C. Harvey, Molecular dynamics simulations on discoidal HDL particles suggest a mechanism for rotation in the apo A-I belt model, J. Mol. Biol. 324 (2002) 703–721.
[52] M.K. Jones, A. Catte, L. Li, J.P. Segrest, Dynamics of activation of lecithin: cholesterol acyltransferase by apolipoprotein A-I, Biochemistry 48 (2009) 11196–11210.
[53] L. Calabresi, G. Franceschini, A. Burkybile, A. Jonas, Activation of lecithin cholesterol acyltransferase by a disulfide-linked apolipoprotein A-I dimer, Biochem. Biophys. Res. Co. 232 (1997) 345–349.
[54] U. Daum, C. Langer, N. Duverger, F. Emmanuel, P. Benoit, P. Denefle, A. Chirazi, P. Cullen, P.H. Pritchard, E. Bruckert, G. Assmann, A. von Eckardstein, Apolipoprotein A-I (R151C)Paris is defective in activation of lecithin: cholesterol acyltransferase but not in initial lipid binding, formation of reconstituted lipoproteins, or promotion of cholesterol efflux, J. Mol. Med. 77 (1999) 614–622.
[55] G. Koukos, A. Chroni, A. Duka, D. Kardassis, V.I. Zannis, Naturally occurring and bioengineered apoA-1 mutations that inhibit the conversion of discoidal to spherical HDL: the abnormal HDL phenotypes can be corrected by treatment with LCAT, Biochem. J. 406 (2007) 167–174.
[56] M. Lee, P.T. Kovanen, G. Tedeschi, E. Oungre, G. Franceschini, L. Calabresi, Apolipoprotein composition and particle size affect HDL degradation by chymase: effect on cellular cholesterol efflux, J. Lipid Res. 44 (2003) 539–546.
[57] L. Calabresi, G. Tedeschi, C. Treu, S. Ronchi, D. Galbiati, S. Airoldi, C.R. Sirtori, Y. Marcel, G. Franceschini, Limited proteolysis of a disulfide-linked apoA-I dimer in reconstituted HDL, J. Lipid Res. 42 (2001) 935–942.
[58] L. Calabresi, G. Vecchio, R. Longhi, E. Gianazza, G. Palm, H. Wadensten, A. Hammarström, A. Olsson, A. Karlström, T. Sejlitz, H. Ageland, C.R. Sirtori, G. Franceschini, Molecular characterization of native and recombinant apolipoprotein A-I_{Milano} dimer: the introduction of an interchain disulfide bridge remarkably alters the physicochemical properties of apolipoprotein A-I, J. Biol. Chem. 269 (1994) 32168–32174.
[59] S. Bhat, M.G. Sorci-Thomas, E.T. Alexander, M.P. Samuel, M.J. Thomas, Intermolecular contact between globular N-terminal fold and C-terminal domain of ApoA-I stabilizes its lipid-bound conformation—studies employing chemical cross-linking and mass spectrometry, J. Biol. Chem. 280 (2005) 33015–33025.
[60] A.K. Behling Agree, M.A. Tricerri, K. Arnvig McGuire, S.M. Tian, A. Jonas, Folding and stability of the C-terminal half of apolipoprotein A-I examined with a Cys-specific fluorescence probe, Biochim. Biophys. Acta 1594 (2002) 286–296.
[61] H.H. Li, D.S. Lyles, W. Pan, E. Alexander, M.J. Thomas, M.G. Sorci-Thomas, ApoA-I structure on discs and spheres. Variable helix registry and conformational states, J. Biol. Chem. 277 (2002) 39093–39101.
[62] C. Arnulphi, S.A. Sanchez, M.A. Tricerri, E. Gratton, A. Jonas, Interaction of human apolipoprotein A-I with model membranes exhibiting lipid domains, Biophys. J. 89 (2005) 285–295.
[63] E.T. Alexander, M. Tanaka, M. Kono, H. Saito, D.J. Rader, M.C. Phillips, Structural and functional consequences of the Milano mutation (R173C) in human apolipoprotein A-I, J. Lipid Res. 50 (2009) 1409–1419.
[64] X.W. Zhu, G. Wu, W.W. Zeng, H. Xue, B.S. Chen, Cysteine mutants of human apolipoprotein A-I: a study of secondary structural and functional properties, J. Lipid Res. 46 (2005) 1303–1311.